Carbon 128 (2018) 117–124

Contents lists available at ScienceDirect

Carbon

journal homepage: www.elsevier.com/locate/carbon

Crumpled graphene prepared by a simple ultrasonic pyrolysis method for fast photodetection

Zhenfei Gao [a, c, 1], Zhiwen Jin [b, 1], Qingqing Ji [c], Yushu Tang [a], Jing Kong [c], Liqiang Zhang [a, *], Yongfeng Li [a, **]

[a] State Key Laboratory of Heavy Oil Processing, China University of Petroleum, Beijing 102249, PR China
[b] Beijing National Laboratory for Molecular Sciences, Key Laboratory of Organic Solids, Institute of Chemistry, Chinese Academy of Sciences, Beijing 100190, PR China
[c] Department of Electrical Engineering and Computer Science, Massachusetts Institute of Technology, Cambridge, MA 02139, USA

ARTICLE INFO

Article history:
Received 29 August 2017
Received in revised form
13 November 2017
Accepted 26 November 2017
Available online 1 December 2017

Keywords:
Graphene
Crumpled
Ultrasonic pyrolysis
Fast
Photodetector

ABSTRACT

In the past decades, graphene has attracted much attention as the host material of photodetectors (PDs), owing to its fascinating mechanical property, ultrahigh carrier mobility and remarkable optical transparency. However, the intrinsic low light absorption of graphene affects its comprehensive application in PDs. Therefore, graphene-based PDs research has focused on hybrid system and optimized graphene structures to enhance photoabsorption. In order to combine the advantages of both approaches, we successfully prepared crumpled reduced graphene oxide (C-rGO) for PDs by a simple ultrasonic pyrolysis method. Through this rapid, one-step capillary-driven route, C-rGO and C-rGO/(ZnO,PbS) composite films can be easily deposited on arbitrary substrates (PET, glass, Al_2O_3 ceramic and paper). Interestingly, the unique C-rGO PDs shows superior stability and fast transient photocurrent response (rise/decay time of 189/189 ms). Furthermore, by incorporating ZnO and PbS nanoparticles to enhance light absorption, the crumpled hybrid nanostructure PDs demonstrate about four times increased photocurrents and broad-band (UV–Vis–NIR) photodetection features with R of 0.12 A/W. Such crumpled C-rGO-based PDs hold great potentials for future optoelectronic applications, and the ultrasonic pyrolysis method could open a new way for engineering novel nanostructured thin films with high-performance photodetection.

1. Introduction

With the rapid technological developments, high performance optoelectronic devices have penetrated into every aspect of our lives, among which, photodetectors (PDs) with the capacity to transform illumination input to an electrical signal output, have been widely used in many fields such as environment monitoring, military, medicine and image display [1–4]. Depending on the mechanisms of the detection, PDs comes from a variety of light sensitive materials and structures, and they offer a wide range of performance metrics such as spectral response, detectivity and response time, etc. With the advent of ubiquitous electronics and internet-of-things, PDs with flexible, portable and low cost, easy deployment features becomes more and more desirable.

Graphene is a potential candidate for such flexible and low cost PDs due to its remarkable optical, electronic, and mechanical properties [5,6], the combination of these properties could meet the development trend of novel optoelectronic devices perfectly [7]. Particularly, graphene's optical absorption spans from UV into far infrared, making it suitable for broadband or IR PDs that very few material systems can be used. Carbon is earth abundant material and the production of graphene can be potentially low cost. Graphene is also chemically very stable, non-toxic, unlike the other materials used for IR detectors such as HgCdTe. Combined with its excellent electrical conduction and remarkable flexibility and mechanical robustness, significant efforts have been devoted to developing graphene-based photodetectors [8–12].

Despite the advantages mentioned above, the intrinsic low light absorption of graphene affects its comprehensive application in PDs. Many efforts have been made to ameliorate this shortcoming. On one hand, researchers achieved higher light absorption by

* Corresponding author.
** Corresponding author.
E-mail addresses: liqiangzhang85@163.com (L. Zhang), yfli@cup.edu.cn (Y. Li).
[1] These authors contributed equally to this work.

https://doi.org/10.1016/j.carbon.2017.11.082
0008-6223/

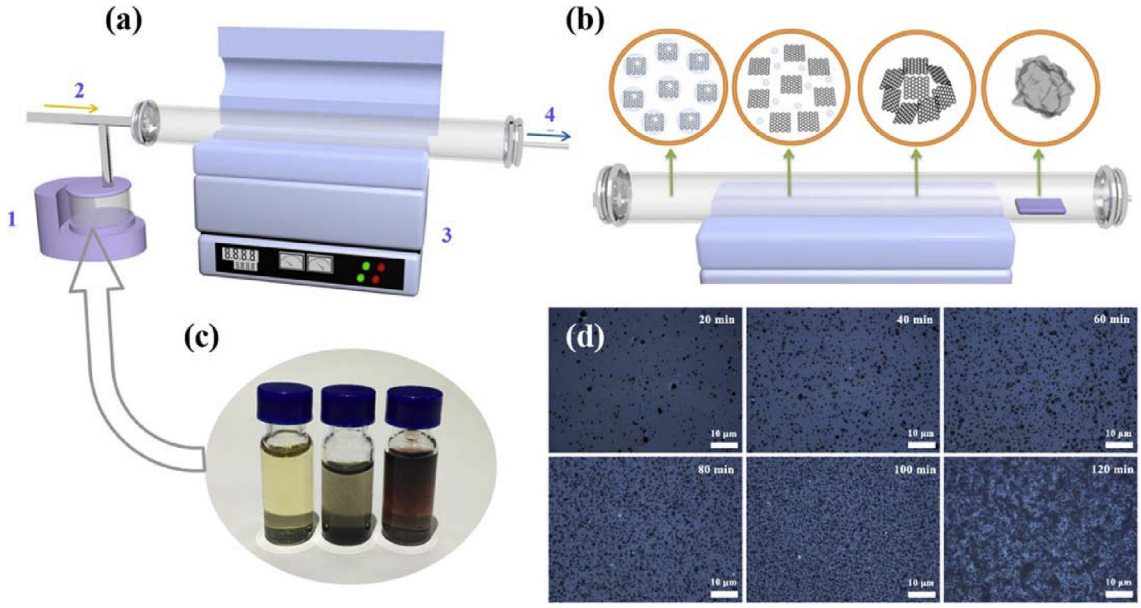

Fig. 1. (a) Schematic diagram of the fabrication apparatus of C-rGO: 1 the ultrasonic atomizer, 2 represents the carrier gas, which is N_2, 3 is the tube furnace, and 4 represents the exhaust gas. (b) Schematic diagram of the formation process of the C-rGO. (c) Microscopic photographs of the GO, GO/ZnO and GO/PbS solution, respectively. (d) Typical optical images of the glass substrate after the C-rGO deposition using different duration of time. (A colour version of this figure can be viewed online.)

optimizing the morphology of the graphene active layer. Kang et al. achieved more than an order-of-magnitude enhancement of the optical extinction by increasing graphene's areal density via a buckled 3D structure [13]. Furchi et al. demonstrated that by monolithically integrating graphene with a Fabry-Pérot microcavity, the optical absorption is 26-fold enhanced [14]. Furthermore, the preparation of a hybrid system is another commonly used method to enhance graphene's light absorption. Shao et al. fabricated a ZnO nanoparticle-graphene core-shell structured ultraviolet photodetector, which showed high responsivity and fast transient response time [15]. Konstantatos et al. demonstrate a hybrid photodetector that consists of graphene covered with a thin film of PbS quantum dots shows a specific detectivity of 7×10^{13} Jones [8]. It is well recognized that the performance of graphene-based PDs could be greatly improved by modifying their morphological features and material compositions [16–20].

In general, graphene could be mainly synthesized through chemical vapor deposition (CVD) [21], mechanical exfoliation [22] and graphene oxide (GO) reduction [23]. Compared with the former two methods, GO reduction has many advantages such as facile experimental conditions, low costs and easy processibility for large scale film fabrication. Since GO can be dissolved in aqueous and alcohol solution, it has been long utilized as the composite material to form novel nanostructures with other photoelectric materials through wet chemistry methods [6,24,25]. Ultrasonic pyrolysis has been widely used to form crumpled graphene nanoparticles from GO solution. The prepared crumpled graphene nanoparticles have many applications in microbial fuel electrodes, supercapacitors, lithium ion battery anodes and metal particle coatings [26–33]. It is anticipated that such C-rGO nanoparticles once processed into a uniform film could scatter and absorb more lights for improved PD performances. Here we report that, by changing atomization sources, the C-rGO nanostructured film can be readily achieved, whose light absorption can be further enhanced by incorporating semiconductor nanoparticles. With a combination of morphological modification and composition tuning, this ultrasonic pyrolysis strategy has shown great promise for graphene-based PDs as will be demonstrated below.

2. Experimental section

2.1. Material preparation

All of the materials were purchased from Sigma-Aldrich Corporation (Shanghai, China) without further treatment. The polyethylene terephthalate (PET), aluminum oxide (Al_2O_3), weighing paper and Corning Eagle XG glass were used as substrates. All substrates were pre-cut into square pieces with a size of 1 cm × 1 cm.

2.2. Solution preparation

Graphene oxide (GO) was fabricated from graphite powder (325 mesh) by a modified Hummer's method [34]. 100 mg GO was dispersed into 100 mL anhydrous ethanol by ultrasonication for 60 min to get a homogeneous alcohol solution.

2.2.1. GO/ZnO solution preparation

0.82 g zinc acetate dissolved into 50 mL methanol contained flask, and continuous magnetic stirring at 60 °C. 0.5 g potassium hydroxide was added into 25 mL methanol and then slowly dropped into the flask. After 3 h, 8-nm-diameter ZnO NPs were obtained. After purification, the obtained ZnO NPs was dispersed in chlorobenzene (1 mg/ml) [35]. 5 mL ZnO solution was added into 100 mL GO NPs solution. The solution was stirred rigorously for 5 h at 60 °C. Then the GO/ZnO nanocomposites solution was obtained.

2.2.2. GO/PbS solution preparation

1.8 g lead oxide (PbO) and 5 mL oleic acid (OA) were added into 50 mL 1-octadecene (ODE) contained flask. After completely dissolved, the solution was ventilation with nitrogen, then heat the solution to 150 °C. Afterwards, the solution was gradually added into the mixture of 0.84 mL hexamethydisilathiane (TMS) and 20 mL ODE, PbS NPs were obtained. Volume ratio of 1:1 isopropyl alcohol: acetone mixture was used to remove excess ions. The obtained PbS NPs was then dispersed in *N*-hexane (1 mg/ml) [36]. 5 mL PbS NPs *N*-hexane solution was added into 100 mL GO NPs

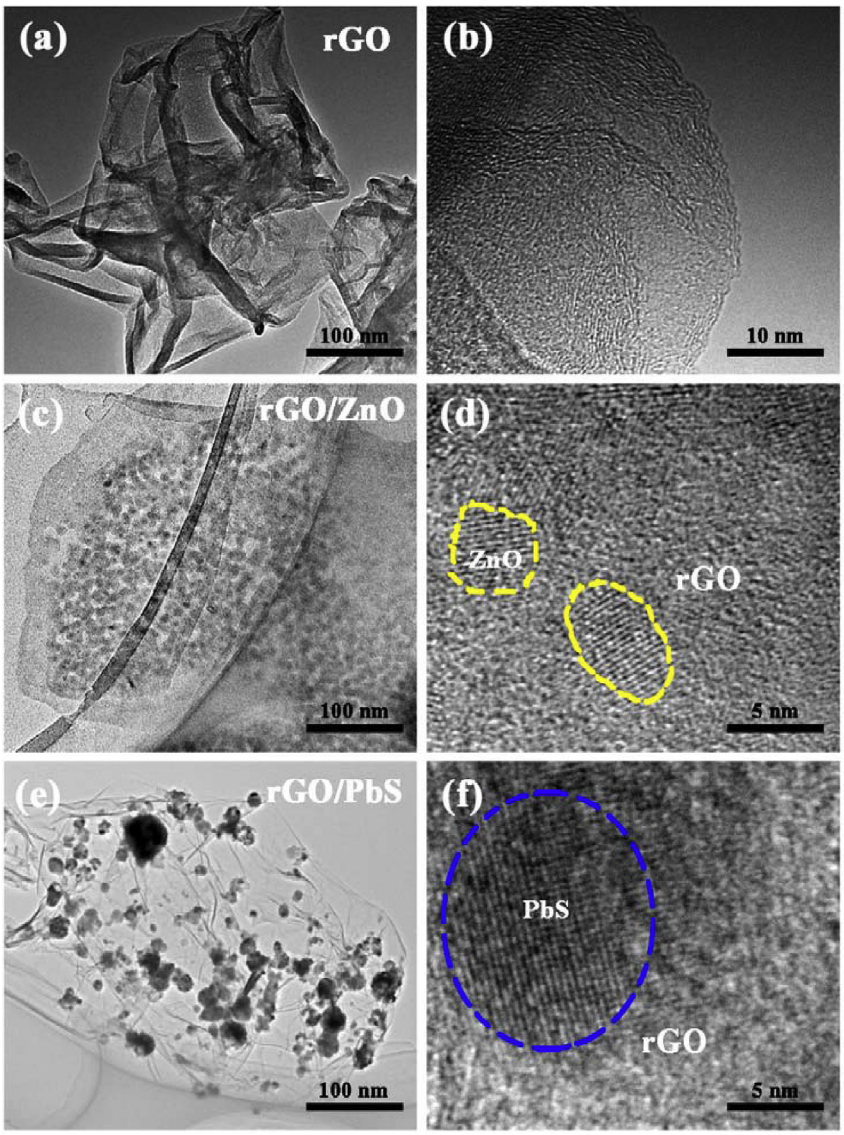

Fig. 2. The TEM images showing the size and existential state of the (a) pristine C-rGO, (c) rGO-wrapped ZnO nanoparticles and (e) rGO-wrapped PbS nanoparticles respectively. (b) The HRTEM image of boundaries of the crumpled graphene. (d), (f): The HRTEM images of rGO/ZnO nanocomposites (d) and rGO/PbS nanocomposites (f). (A colour version of this figure can be viewed online.)

solution. The solution was stirred rigorously for 5 h at 60 °C. Then the GO/PbS nanocomposites solution was obtained.

2.3. Device fabrication

The C-rGO and hybrid C-rGO/(ZnO, PbS) films were both fabricated via ultrasonic pyrolysis method. The activity layers were directly formed on various substrates placed in the rear cold part of the furnace quarts tube. After the films were prepared, the device was completed with the thermal evaporation of 100 nm-thick Ag/WO3/Ag transparent electrodes through shadow masks resulting in a channel width/length of 2000/5 μm.

2.4. Characterization

Surface morphology of C-rGO deposited on the glass substrate was identified by using the FEI Quanta 200F scanning electron microscope (SEM), which is operated at a voltage of 30 kV. The X-ray photoelectron spectroscopy (XPS, Thermo Fisher K-Alpha American with an Al Kα X-ray source) was used to measure the elemental composition of rGO. The structure of the crumpled graphene and hybrid C-rGO/ZnO and C-rGO/PbS were investigated by using the FEI Tecnai G2 F20 transmission electron microscopy (TEM) operated at 200 kV. The TEM analyses included the common TEM images at a low magnification and high-resolution transmission electron microscopy (HRTEM) images. The AFM images were carried out by using a Veeco NanoScope IV with a silicon cantilever in tapping mode. The Keithley 4200 and a Micromanipulator 6150 probe station were used to record all the electrical characterization at room temperature in air. UV–vis spectra were recorded using JASCO V-570 spectrophotometer. The UPS analysis was performed in a KRATOS ULTRA AXIS DLD photoelectron spectroscopy system with an unfiltered He I (21.22 eV) gas-discharge lamp. With an excitation wavelength of 532 nm, Raman spectroscopy was implemented by using a micro-Raman spectrometer (InVia Reflex, Renishaw, UK). A 100× objective lens was used in the Raman measurement with a numerical aperture (NA) of 0.95. All peaks in the Raman spectra were fitted with Lorentzians.

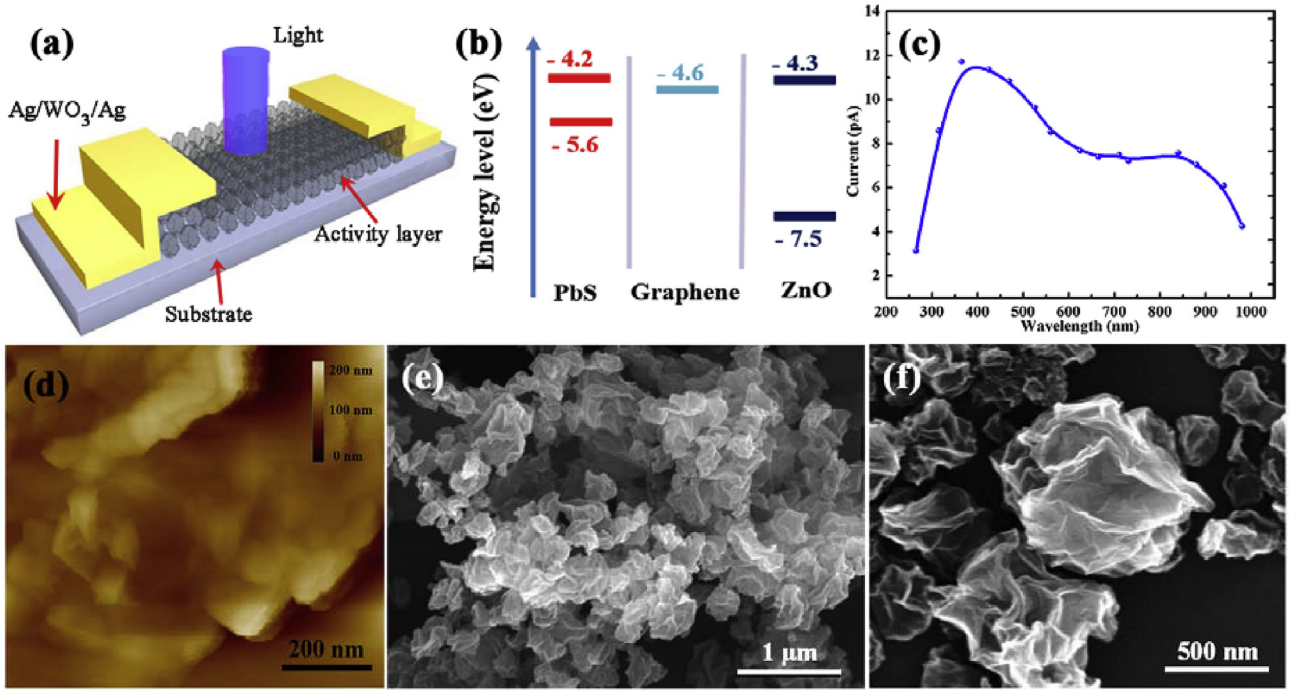

Fig. 3. (a) Schematic illustration of the crumpled graphene based photodetector. (b) Energy level diagram of ZnO, PbS and graphene. (c) The light current spectral of crumpled C-rGO/PbS film (Light density of 1 μW/cm^2). (d) AFM image of the C-rGO film on glass substrate. (e) Low magnification and (f) high magnification SEM images of C-rGO exhibit the morphology of the fabricated crumpled graphene film. (A colour version of this figure can be viewed online.)

3. Results and discussion

The details of C-rGO nanoparticles preparation schematic is illustrated in Fig. 1a [31]. 100 mL pre-fabricated GO alcohol solution was poured into an ultrasonic atomizer marked with **label 1**. The nebulized GO aerosol droplets were carried by 1 L/min N_2 gas from a steel tube (**label 2**, yellow arrow indicates the airflow direction) and flew through a preheated 550 °C tube furnace shown as **label 3**. The GO aerosol droplets gradually evolved into C-rGO nanoparticles and deposited into a thin film at the cold rear part of the quartz tube. Fig. 1b shows the formation process of C-rGO nanoparticles comprising ethanol evaporation, thermal reduction of GO aerosol droplets, and film evolution on any substrates placed 5-cm away from the furnace. The **label 4** marks the exhaust gas discharged into a collection device, with blue arrow indicating the exhaust gas direction. Fig. 1d shows the typical optical images of the fabricated C-rGO films as a function of the deposition time. Hybrid rGO-based devices can be conveniently prepared via the same method by using the GO/ZnO and GO/PbS mixed solutions pre-synthesized as the atomization sources, respectively. Fig. 1c shows the microscopic photographs of the prepared GO, GO/ZnO and GO/PbS solution, respectively.

The prepared C-rGO nanoparticles and the hybrid C-rGO/ZnO and C-rGO/PbS nanoparticles were characterized by transmission electron microscopy (TEM), as shown in Fig. 2a, c and e, respectively. The well-folded morphology of a single C-rGO nanoparticle can be obviously identified in Fig. 2a, and the average diameter of the C-rGO nanoparticles is about 200 nm. Fig. 2b reveals the edge of C-rGO formed by stacked rGO nanosheets, indicating their ultra-thinness. As shown in Fig. 2c and e, the sizes of the hybrid C-rGO/ZnO and C-rGO/PbS nanoparticles are a little larger than that of the pristine C-rGO nanoparticle due to the embedment of the semiconducting nanoparticles, which can be clearly distinguished from the reduced graphene oxide (rGO) with the atomic fringes (Fig. 2d and f, respectively). The folding process of the graphene sheets may be accordingly affected, resulting in larger sizes for the hybrid C-rGO nanoparticles.

A conceptual schematic of the C-rGO-based photodetector is illustrated in Fig. 3a. The 100 nm-thick Ag/WO_3/Ag transparent electrodes were obtained by thermal evaporation on the photoactive layer through shadow masks [37]. The transmission properties of the hybrid C-rGO/ZnO PDs is given in Fig. S1 with almost constant transparency of around 80% in the visible range (380–780 nm) and of <80% in the lower wavelength range (<400 nm). The inset of Fig. S1 is an optical photograph of the crumpled C-rGO/ZnO film deposited on a quartz substrate, which clearly demonstrates the remarkable transparency and having little influence on observing the flowers underneath. The energy level diagrams of graphene, ZnO and PbS are shown in Fig. 3b. The spectral based light current plot for C-rGO/PbS film is further presented in Fig. 3c. The AFM height image of the C-rGO particles is given in Fig. 3d. Fig. 3e and f shows the SEM images of C-rGO film deposited on the glass substrate under low magnification and high magnification, respectively (the SEM images of a series of magnifications are demonstrated in Fig. S2). All these images give consistent sizes of ~200 nm for the C-rGO nanoparticles. The crumpled morphology of rGO is more obviously exhibited in Fig. 3f with a large-size C-rGO nanoparticle of ~500 nm in diameter. X-ray photoelectron spectroscopy (XPS) analysis in Fig. 4a provides the detailed information about the C 1s signals of the as prepared C-rGO. The peaks at 284.6, 285.2, 285.9 and 289.2 eV are corresponding to C–C, C–N, C–O and O=C–O, respectively [38]. Furthermore, Raman spectra of the C-rGO film displays two significant peaks at around 1357 and 1590 cm^{-1} (Fig. 4b), which are related to the D band and G band, respectively [39].

Four types of substrates have been selected to evolve the C-rGO films, which are polyethylene terephthalate (PET), aluminum oxide (Al_2O_3), weighing paper and Corning Eagle XG glass, respectively. Fig. 5a shows the typical *I*–*V* characteristics of C-rGO films deposited on the four substrates in dark and under illumination with an

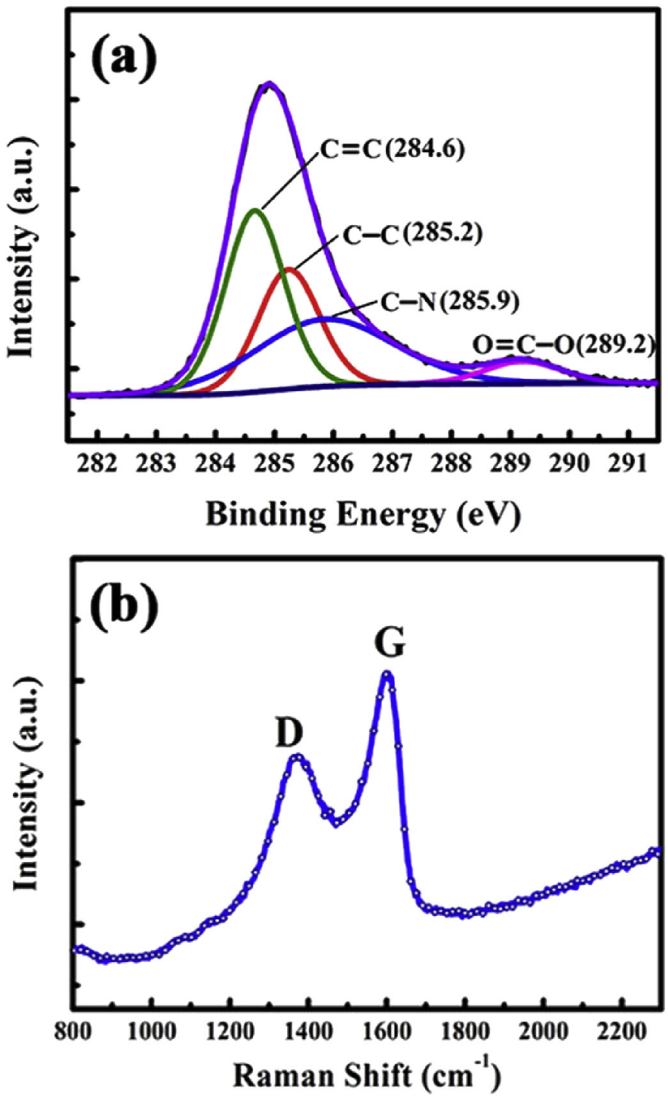

Fig. 4. (a) XPS spectra of the C-rGO. (b) The Raman spectrum of C-rGO. (A colour version of this figure can be viewed online.)

incident of 1 μW/cm^2 at 365 nm. When the C-rGO is illuminated under UV light, electron-hole pairs are generated and further separated with the existence of the bias, resulting in an increased current through the C-rGO channel [24]. The optical rise/decay information of C-rGO film is presented in Fig. 5b at a bias of 10 V. The current rises rapidly upon illumination and decays within nearly the same time (~189 ms) after turning off the light (the rise time was defined as the time for the current increased to 90% of the peak value and the decay time was defined as the time for the current decreased to 10% of the peak value) [40]. Fig. 5c–f demonstrate the on/off switching characteristics of C-rGO film deposited on the four different substrates under a bias of 10 V, and the on/off time duration is 10/10 s. All the four devices show excellent on/off switching repeatability and stability. It is interesting to find that rougher substrates exhibited higher photocurrents, probably associated with the longer light path on such surfaces.

Hybrid rGO-based devices can be conveniently prepared via the same method by using the GO/ZnO and GO/PbS mixed solutions pre-synthesized as the atomization sources, respectively. The performances of the fabricated devices based on C-rGO/ZnO and C-rGO/PbS films deposited on glass substrates are also presented in Fig. 6a under the incident light intensity of 1 μW/cm^2 and at dark under a fixed bias of 10 V. The UV–visible absorption spectra of C-rGO, ZnO and PbS films (all on quarts substrates) are shown in Fig. 6b. It is found that ZnO film mainly absorbs light in the UV region (peaks at ~345 nm) and PbS film has light absorption peaked at the near infrared region (~950 nm). The current responses of C-rGO/ZnO film and C-rGO/PbS film in Fig. 6c and e demonstrate an increase of a few times after incorporation of these semiconducting nanoparticles, which can absorb incident light more efficiently. Fig. 6d and f presents the light rise/decay information of the crumpled C-rGO/ZnO film and crumpled C-rGO/PbS film, both of which are around 390 ms and two orders of magnitude faster than the ZnO-based UV PDs [41]. To compare the performance of C-rGO and C-rGO/(ZnO, PbS) more intuitively, the I–V curves of the C-rGO, C-rGO/ZnO and C-rGO/PbS films were measured in the dark and under 365 nm UV light. It can be clearly seen in Fig. S3a that the photocurrent of C-rGO/ZnO and C-rGO/PbS both show tenfold increase under UV light illumination. Fig. S3b shows the absorption spectrum of the pristine C-rGO, the hybrid C-rGO/ZnO and C-rGO/PbS films. It is found that the C-rGO/ZnO and C-rGO/PbS films have the similar absorption peak as the ZnO and PbS films. According to the following Eq. (1):

$$R = \frac{I_{Light} - I_{Dark}}{P_{ill}} \quad (1)$$

where I_{Light} is current under light illumination, I_{Dark} the dark current, P_{ill} the incident illumination power on the effective area (channel area), R the photoresponsivity, the best R (0.12 A/W) is achieved upon device optimization. The detectivity (D*, in units of Jones to characterize the sensitivity) is another figure of merits used for evaluating the photoconductor performance. The D* can be expressed by the following Eq. (2):

$$D* = R\sqrt{\frac{S}{2qI_{dark}}} \quad (2)$$

where S is the effective area under illumination, q is the electron charge, I_{Dark} is the dark current. The detectivity is 1.4×10^{12} Jones upon the previously calculated photoresponsivity (R = 0.12 A/W). Fig. S4a–c demonstrates the photocurrent versus time under different UV light illumination intensities of C-rGO, C-rGO/ZnO and C-rGO/PbS film under a bias of 10 V. It can be obviously seen that all prepared films show great photocurrent responses sensitivity to the illustration UV light intensity. In Fig. S4d, the linear dynamic range (LDR) of pristine C-rGO, the hybrid C-rGO/ZnO and C-rGO/PbS films were measured under UV light.

The fast transient response of C-rGO/ZnO and C-rGO/PbS PDs in our work can be comprehended by analyzing the carrier transport processes. The energy level diagrams of graphene, ZnO and PbS are shown in Fig. 3b. The electron affinity for ZnO and PbS are 4.3 and 4.2 eV, respectively. Meanwhile, graphene's work function is known to be 4.6 eV [42]. In our hybrid semiconductor/rGO structures, the semiconductor is well-contacted with graphene. Upon UV illumination, it is energetically beneficial for photogenerated electrons being transferred from the conduction bands of these two semiconductor materials to the graphene. Due to the high carrier mobility of graphene, electrons transferred to the graphene side show less accumulation. Therefore, the carrier transport efficiency can be significantly improved in the crumpled semiconductor/rGO structures and the fast rise of photocurrent is carried out. After turning off the UV light, the redundant photocarriers are quickly conducted away, leading to a fast decay time [15]. The existence of

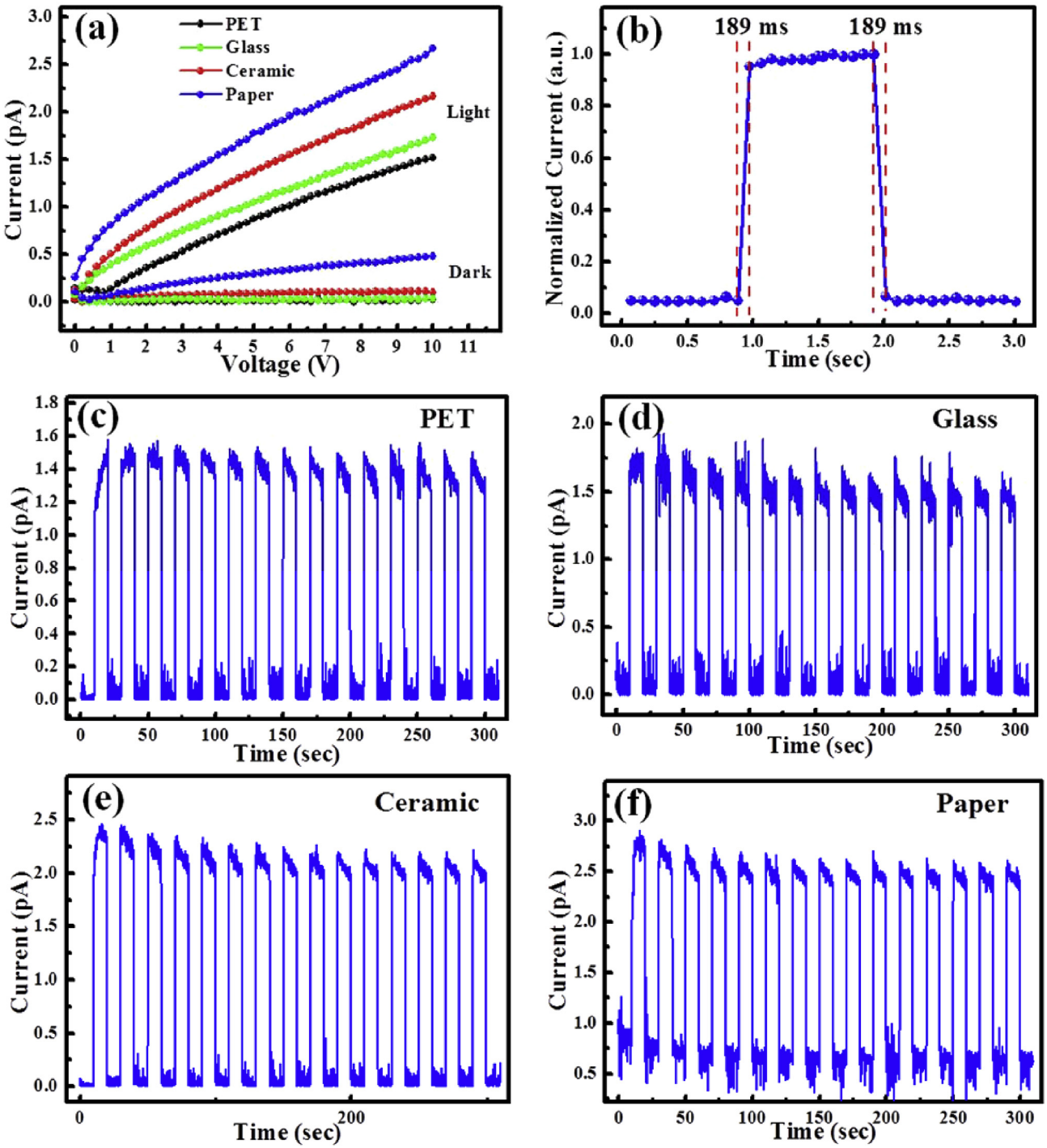

Fig. 5. (a) I–V characteristics of the pristine C-rGO in the dark and under incident illumination at 365 nm with 1 μW/cm^2. (b) Rise/decay time comparison under a bias of 10 V. On-off switching property of C-rGO films deposited on (c) the PET, (d) the glass, (e) the Al_2O_3 and (f) the paper substrate. (A colour version of this figure can be viewed online.)

ZnO and PbS nanoparticles in the hybrid crumpled graphene nanostructure plays a very important role in increasing the photocurrent. Nonetheless, the rise/decay time of C-rGO/ZnO and C-rGO/PbS films are much slower than the C-rGO film. When the C-rGO/ZnO and C-rGO/PbS films under light illumination, the generated electron and hole pairs in ZnO and PbS will transfer to graphene due to the lower energy level of electrons and holes in graphene. However, the transfer rates of electrons and holes are quite different in ZnO, PbS nanoparticles and in graphene. In consequences, the relatively slow transfer rates of electrons and holes in ZnO and PbS leads to the slower rise/decay time of C-rGO/ZnO and C-rGO/PbS films. It is widely accepted that the performance of ZnO-based UV detector can be affected easily by the slow absorption and desorption processes of oxygen molecules on the ZnO surface [43], resulting in long rise and decay times. Here, the crumpled rGO component can efficiently shorten the rise/decay time of ZnO nanoparticles to decrease the effect of oxygen adsorption on the ZnO based photodetector.

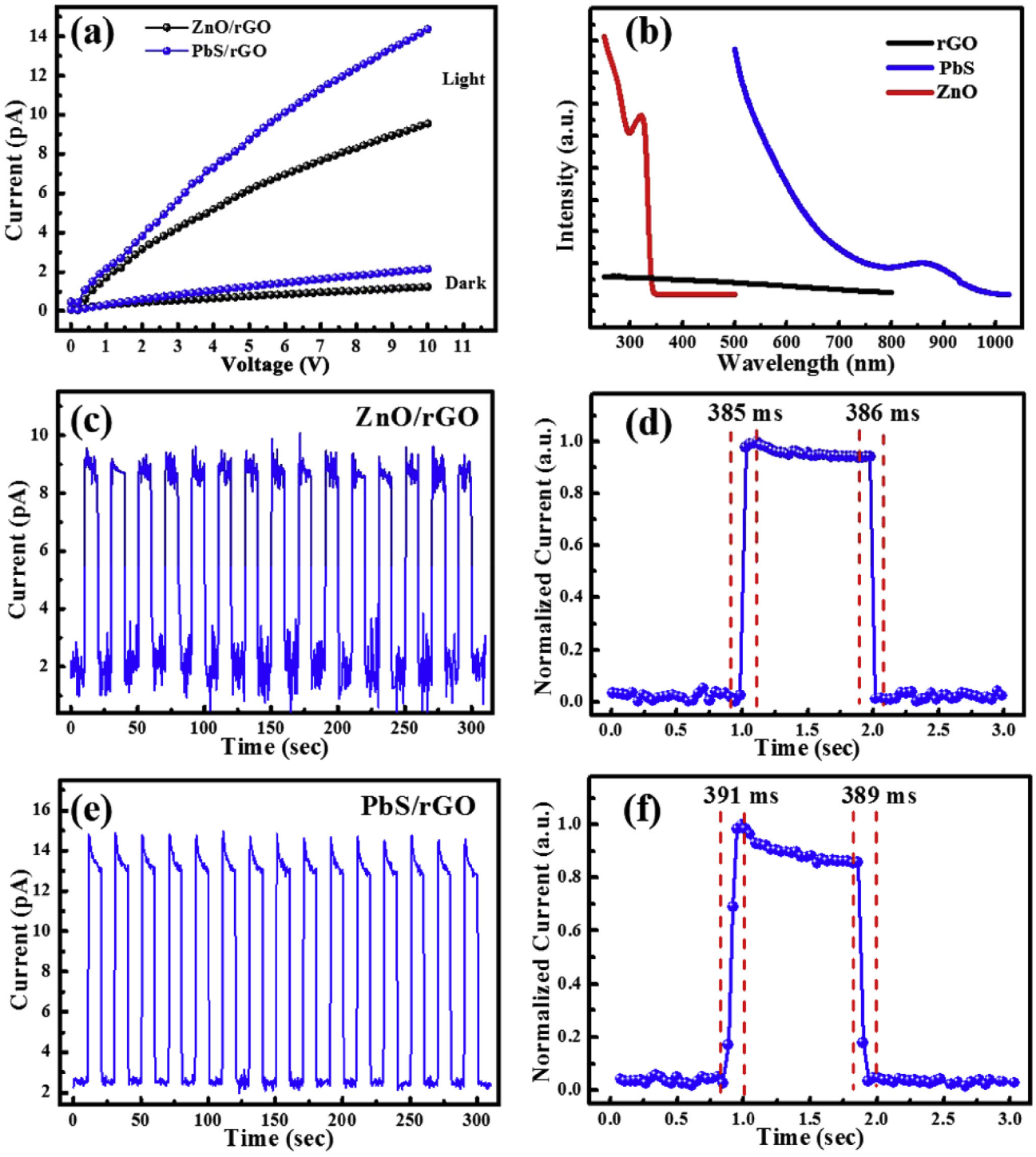

Fig. 6. (a) I–V curves of the hybrid C-rGO/ZnO and C-rGO/PbS film in the dark and under 365 nm UV light. (b) Absorption spectrum of the pristine C-rGO, the fabricated ZnO and PbS particles. On-off switching properties and rise/decay time measurement: (c) and (d) for a C-rGO/ZnO device, (e) and (f) for a C-rGO/PbS device. (A colour version of this figure can be viewed online.)

4. Conclusion

In conclusion, the novel C-rGO-based films were successfully synthesized on different types of substrates by a simple ultrasonic pyrolysis method. Fully transparent PDs have also been fabricated after deposition of the Ag/WO_3/Ag electrodes, demonstrating ultrafast rise/decay responses (rise/decay time of 189/189 ms) and outstanding stability. Furthermore, after incorporation of ZnO and PbS nanoparticles, the crumpled hybrid nanostructure PDs demonstrates ten-fold increase in the photocurrent, along with non-degraded response time and stability. Meanwhile, the C-rGO/PbS based PDs exhibits remarkable photodetection in the broad UV–Vis–NIR range with optimized R of 0.12 A/W. We believe that the rGO-based PDs could have diverse applications in future optoelectronics. And the ultrasonic pyrolysis method could open a new way for the preparation of novel nano-morphology thin films

and high-performance graphene-based photoelectrical devices.

Competing financial interests

The authors declare no competing financial interests.

Acknowledgements

This work was financially supported by the National Natural Science Foundation of China (No. 21576289, 51401239, 21776308), Science Foundation of China University of Petroleum, Beijing (No. C201603), Science Foundation Research Funds Provided to New Recruitments of China University of Petroleum, Beijing (2462014QZDX01) and Thousand Talents Program.

Appendix A. Supplementary data

Supplementary data related to this article can be found at https://doi.org/10.1016/j.carbon.2017.11.082.

References

[1] S. Pang, S. Yang, X. Feng, K. Müllen, Coplanar asymmetrical reduced graphene oxide–titanium electrodes for polymer photodetectors, Adv. Mater. 24 (12) (2012) 1566–1570.
[2] H. Chen, H. Liu, Z. Zhang, K. Hu, X. Fang, Nanostructured photodetectors: from ultraviolet to terahertz, Adv. Mater. 28 (3) (2016) 403–433.
[3] H. Chang, H. Wu, Graphene-based nanomaterials: synthesis, properties, and optical and optoelectronic applications, Adv. Funct. Mater. 23 (16) (2013) 1984–1997.
[4] F. Koppens, T. Mueller, P. Avouris, A. Ferrari, M. Vitiello, M. Polini, Photodetectors based on graphene, other two-dimensional materials and hybrid systems, Nat. Nanotechnol. 9 (10) (2014) 780–793.
[5] S. Jang, E. Hwang, Y. Lee, S. Lee, J.H. Cho, Multifunctional graphene optoelectronic devices capable of detecting and storing photonic signals, Nano Lett. 15 (4) (2015) 2542–2547.
[6] H. Chang, Z. Sun, Q. Yuan, F. Ding, X. Tao, F. Yan, et al., Thin film field-effect phototransistors from bandgap-tunable, solution-processed, few-layer reduced graphene oxide films, Adv. Mater. 22 (43) (2010) 4872–4876.
[7] J. Li, L. Niu, Z. Zheng, F. Yan, Photosensitive graphene transistors, Adv. Mater. 26 (31) (2014) 5239–5273.
[8] G. Konstantatos, M. Badioli, L. Gaudreau, J. Osmond, M. Bernechea, F.P.G. De Arquer, et al., Hybrid graphene-quantum dot phototransistors with ultrahigh gain, Nat. Nanotechnol. 7 (6) (2012) 363–368.
[9] Ling X, Lin Y, Ma Q, Kong J, Dresselhaus M. Synthesis and Photoresponse of the Graphene-MoS2 in-plane Heterostructures. APS Meeting Abstracts.
[10] F. Xia, T. Mueller, Y.-M. Lin, A. Valdes-Garcia, P. Avouris, Ultrafast graphene photodetector, Nat. Nanotechnol. 4 (12) (2009) 839–843.
[11] T. Mueller, F. Xia, P. Avouris, Graphene photodetectors for high-speed optical communications, Nat. Photon. 4 (5) (2010) 297–301.
[12] Y. Zhang, T. Liu, B. Meng, X. Li, G. Liang, X. Hu, et al., Broadband high photoresponse from pure monolayer graphene photodetector, Nat. Commun. 4 (2013) 1811.
[13] P. Kang, M.C. Wang, P.M. Knapp, S. Nam, Crumpled graphene photodetector with enhanced, strain-tunable, and wavelength-selective photoresponsivity, Adv. Mater. 28 (23) (2016) 4639–4645.
[14] M. Furchi, A. Urich, A. Pospischil, G. Lilley, K. Unterrainer, H. Detz, et al., Microcavity-integrated graphene photodetector, Nano Lett. 12 (6) (2012) 2773–2777.
[15] D. Shao, M. Yu, H. Sun, T. Hu, S. Sawyer, High responsivity, fast ultraviolet photodetector fabricated from ZnO nanoparticle–graphene core–shell structures, Nanoscale 5 (9) (2013) 3664–3667.
[16] R.-J. Shiue, Y. Gao, Y. Wang, C. Peng, A.D. Robertson, D.K. Efetov, et al., High-responsivity graphene–boron nitride photodetector and autocorrelator in a silicon photonic integrated circuit, Nano Lett. 15 (11) (2015) 7288–7293.
[17] T. Yu, F. Wang, Y. Xu, L. Ma, X. Pi, D. Yang, Graphene coupled with silicon quantum dots for high-performance bulk-silicon-based schottky-junction photodetectors, Adv. Mater. 28 (24) (2016) 4912–4919.
[18] W.C. Tan, W.H. Shih, Y.F. Chen, A highly sensitive graphene-organic hybrid photodetector with a piezoelectric substrate, Adv. Funct. Mater. 24 (43) (2014) 6818–6825.
[19] K.K. Manga, J. Wang, M. Lin, J. Zhang, M. Nesladek, V. Nalla, et al., High-performance broadband photodetector using solution-processible PbSe–TiO2–graphene hybrids, Adv. Mater. 24 (13) (2012) 1697–1702.
[20] S. Liu, Q. Liao, S. Lu, Z. Zhang, G. Zhang, Y. Zhang, Strain modulation in graphene/ZnO nanorod film schottky junction for enhanced photosensing performance, Adv. Funct. Mater. 26 (9) (2016) 1347–1353.
[21] M. Losurdo, M.M. Giangregorio, P. Capezzuto, G. Bruno, Graphene CVD growth on copper and nickel: role of hydrogen in kinetics and structure, Phys. Chem. Chem. Phys. 13 (46) (2011) 20836–20843.
[22] A.K. Geim, K.S. Novoselov, The rise of graphene, Nat. Mater 6 (3) (2007) 183–191.
[23] D.R. Dreyer, S. Park, C.W. Bielawski, R.S. Ruoff, The chemistry of graphene oxide, Chem. Soc. Rev. 39 (1) (2010) 228–240.
[24] B. Chitara, S. Krupanidhi, C. Rao, Solution processed reduced graphene oxide ultraviolet detector, Appl. Phys. Lett. 99 (11) (2011), 113114.
[25] B. Chitara, L. Panchakarla, S. Krupanidhi, C. Rao, Infrared photodetectors based on reduced graphene oxide and graphene nanoribbons, Adv. Mater. 23 (45) (2011) 5419–5424.
[26] X. Ma, M.R. Zachariah, C.D. Zangmeister, Crumpled nanopaper from graphene oxide, Nano Lett. 12 (1) (2011) 486–489.
[27] B.S. Mao, Z. Wen, Z. Bo, J. Chang, X. Huang, J. Chen, Hierarchical nanohybrids with porous CNT-networks decorated crumpled graphene balls for supercapacitors, ACS Appl. Mater Interfaces 6 (12) (2014) 9881–9889.
[28] S. Mao, Z. Wen, H. Kim, G. Lu, P. Hurley, J. Chen, A general approach to one-pot fabrication of crumpled graphene-based nanohybrids for energy applications, ACS Nano 6 (8) (2012) 7505–7513.
[29] S.H. Choi, Y.C. Kang, Fe 3 O 4-decorated hollow graphene balls prepared by spray pyrolysis process for ultrafast and long cycle-life lithium ion batteries, Carbon 79 (2014) 58–66.
[30] J.Y. Lee, K.H. Lee, Y.J. Kim, J.S. Ha, S.S. Lee, J.G. Son, Sea-urchin-inspired 3D crumpled graphene balls using simultaneous etching and reduction process for high-density capacitive energy storage, Adv. Funct. Mater. 25 (23) (2015) 3606–3614.
[31] J. Luo, H.D. Jang, T. Sun, L. Xiao, Z. He, A.P. Katsoulidis, et al., Compression and aggregation-resistant particles of crumpled soft sheets, ACS Nano 5 (11) (2011) 8943–8949.
[32] J. Luo, X. Zhao, J. Wu, H.D. Jang, H.H. Kung, J. Huang, Crumpled graphene-encapsulated Si nanoparticles for lithium ion battery anodes, J. Phys. Chem. Lett. 3 (13) (2012) 1824–1829.
[33] S.W. Cranford, M.J. Buehler, Packing efficiency and accessible surface area of crumpled graphene, Phys. Rev. B 84 (20) (2011), 205451.
[34] W.S. Hummers Jr., R.E. Offeman, Preparation of graphitic oxide, J. Am. Chem. Soc. 80 (6) (1958) 1339.
[35] W.J. Beek, M.M. Wienk, M. Kemerink, X. Yang, R.A. Janssen, Hybrid zinc oxide conjugated polymer bulk heterojunction solar cells, J. Phys. Chem. B 109 (19) (2005) 9505–9516.
[36] M.A. Hines, G.D. Scholes, Colloidal PbS nanocrystals with size-tunable near-infrared emission: observation of post-synthesis self-narrowing of the particle size distribution, Adv. Mater. 15 (21) (2003) 1844–1849.
[37] Z. Qi, J. Cao, L. Ding, J. Wang, Transparent and transferrable organic optoelectronic devices based on WO3/Ag/WO3 electrodes, Appl. Phys. Lett. 106 (5) (2015) 14_1.
[38] Y. Ping, J.-M. Yan, Z.-L. Wang, H.-L. Wang, Q. Jiang, Ag 0.1-Pd 0.9/rGO: an efficient catalyst for hydrogen generation from formic acid/sodium formate, J. Mater. Chem. A 1 (39) (2013) 12188–12191.
[39] A. Ferrari, J. Meyer, V. Scardaci, C. Casiraghi, M. Lazzeri, F. Mauri, et al., Raman spectrum of graphene and graphene layers, Phys. Rev. Lett. 97 (18) (2006), 187401.
[40] W. Tian, T. Zhai, C. Zhang, S.L. Li, X. Wang, F. Liu, et al., Low-cost fully transparent ultraviolet photodetectors based on electrospun ZnO-SnO2 heterojunction nanofibers, Adv. Mater. 25 (33) (2013) 4625–4630.
[41] Y. Jin, J. Wang, B. Sun, J.C. Blakesley, N.C. Greenham, Solution-processed ultraviolet photodetectors based on colloidal ZnO nanoparticles, Nano Lett. 8 (6) (2008) 1649–1653.
[42] Y.-J. Yu, Y. Zhao, S. Ryu, L.E. Brus, K.S. Kim, P. Kim, Tuning the graphene work function by electric field effect, Nano Lett. 9 (10) (2009) 3430–3434.
[43] Z. Jin, Q. Zhou, Y. Chen, P. Mao, H. Li, H. Liu, et al., Graphdiyne: ZnO nanocomposites for high-performance UV photodetectors, Adv. Mater. 28 (19) (2016) 3697–3702.